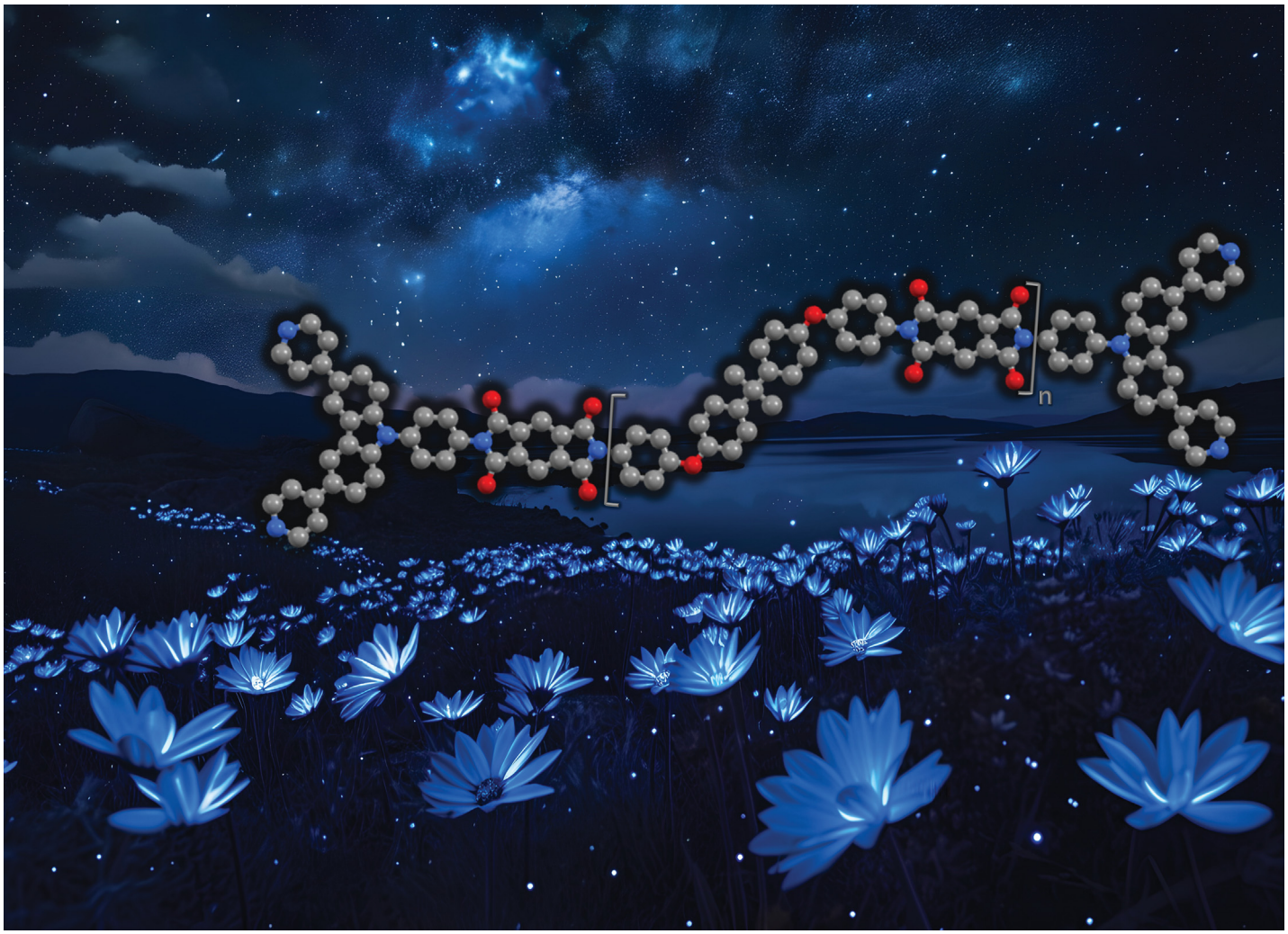

Showcasing a shining example of collaboration between an academic research team and a commercial company towards new emissive materials.

Deep-blue emissive and colourless polyimides: optical property tuning by triphenylamino and carbazole chromophores

Planarization of chromophoric comonomers as an efficient way to achieve transparent and colourless yet deep-blue emissive polyimide films.

As featured in:

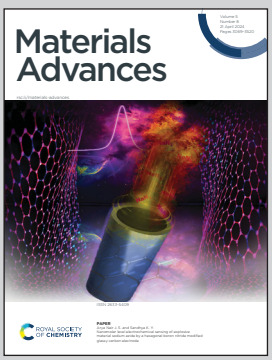

See Jiří Tydlitát *et al.*, *Mater. Adv.*, 2024, **5**, 3198.

ROYAL SOCIETY OF CHEMISTRY

rsc.li/materials-advances

Registered charity number: 207890

Materials Advances

ROYAL SOCIETY OF CHEMISTRY

PAPER

View Article Online
View Journal | View Issue

Cite this: *Mater. Adv.*, 2024, 5, 3198

Deep-blue emissive and colourless polyimides: optical property tuning by triphenylamino and carbazole chromophores†

Pavel Šimon,[ab] Jakub Štrojsa,[a] Milan Klikar,[a] Zuzana Burešová,[a] Aleš Růžička,[c] Jiří Zelenka,[b] Jiří Kulhánek[a] and Jiří Tydlitát*[a]

Received 17th October 2023,
Accepted 9th January 2024

DOI: 10.1039/d3ma00871a

rsc.li/materials-advances

Two novel emissive chromophores based on triphenylamine and carbazole have been designed, prepared and further utilized as comonomers towards end-capped emissive colourless polyimides. The polyimide films were fabricated using 1,2,4,5-cyclohexanetetracarboxylicdianhydride/2,2-bis[4-(4-aminophenoxy)phenyl]propane (CHDA-BAPP) and 4,4′-(hexafluoroisopropylidene)diphthalic anhydride/2,2′-bis(trifluoromethyl)benzidine (6FDA-TFMB), and 5, 1 or 0.1 mol% of comonomer. Fundamental structure–property relationships were elucidated both in solution and the polymeric backbone. Facile planarization/rigidification of the chromophore central donor turned out to be a useful strategy to modulate the optical and thermal properties both of the single molecule and polymeric film. The prepared films are highly thermally stable ($T^{5\%}$ up to 526 °C) and highly transparent (T^{400} ranging between 72–86% for 0.1 mol% loadings), and most of the films were colourless. The luminescence colour of the films ranges from yellow-greenish to blue. CHDA-BAPP carbazole-terminated PIs showed deep-blue emission and excellent optical properties with $CIE_y \leq 0.1$ and high colour purity (FWHM 38 resp. 42 nm) doped with 1 resp. 0.1 mol% of comonomer. The experimental data were further corroborated by DFT calculations and single crystal X-ray analysis.

Introduction

A tremendous number of emissive materials have been developed and found commercial applications across various fields. Yet, with endless technology development, these materials with tailored properties are very challenging and at the centre of interest. Emissive chromophores and polymers have wide potential applications in organic electronics; push–pull chromophores containing triphenylamine (TPA) or a carbazole moiety are particular examples. These emissive derivatives have found various applications in organic photovoltaics (OPVs)[1] as, for example, luminescent solar concentrators (LSCs)[2,3] and organic light emitting diodes (OLEDs),[4–7] but also in the field of sensing of biological processes.[8–11] TPA- and carbazole-derived chromophores have been extensively studied for their pronounced properties, such as aggregation induced emission (AIE),[4,7,12] dual fluorescence,[13] thermally activated delayed fluorescence (TADF),[14] mechanofluorochromism[7,15] *etc.* Peculiar optical properties impart TPA and carbazole derivatives with the potential to be applied in organic electronics and sensing materials, especially as the emissive part of a polymeric backbone. Polyimide (PI) is a typical example due to its high thermal stability and thus suitability for space applications.[16] Besides thermal robustness, optical transparency is often a required parameter of emissive PI films.[17,18] Some emissive PIs containing TPA subunits[19–21] and featuring electrochromic[22,23] or luminescent[24] properties have been described.

Based on our previous work on emissive TPA derivatives,[25,26] we report herein a facile synthesis of novel TPA and carbazole derivatives **1** and **2** (Fig. 1) that were further used as

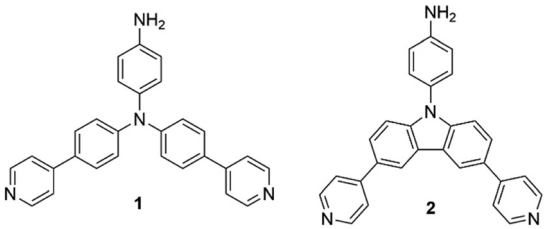

Fig. 1 Two novel TPA- and carbazole-derived chromophoric comonomers.

[a] *Institute of Organic Chemistry and Technology, Faculty of Chemical Technology, University of Pardubice, Studentská 573, Pardubice 53210, Czech Republic. E-mail: jiri.tydlitat@upce.cz*
[b] *Toseda s.r.o., U Panasonicu 376, Staré Čivice, Czech Republic*
[c] *Department of General and Inorganic Chemistry, Faculty of Chemical Technology, University of Pardubice, Studentská 573, Pardubice, 532 10, Czech Republic*

† Electronic supplementary information (ESI) available: Syntheses, NMR, HR-MS, thermal properties, electrochemistry, DFT calculations, and films. CCDC 2206624. For ESI and crystallographic data in CIF or other electronic format see DOI: https://doi.org/10.1039/d3ma00871a

chromophoric comonomers to prepare fluorescent PIs. These push–pull molecules possess a D–π–D–$(\pi–A)_2$ arrangement with two pyridine acceptors and one central amino donor (TPA or carbazole) equipped with a free amino group at the third branch. The latter allows **1** and **2** to be used as reactive comonomers affording emissive PI films.

Results and discussion

Comonomers

Synthesis. Emissive TPA and carbazole comonomers **1** and **2** were obtained in a three-step reaction, and both comonomers were isolated in 61 and 22% overall yields. The first step involved nucleophilic substitution of 1-fluoro-4-nitrobenzene with an appropriate amine **3** or **6** (Scheme 1). Two peripheral pyridyls were introduced *via* subsequent two-fold Suzuki–Miyaura cross-couplings with pyridin-4-ylboronic acid. Target amines **1** and **2** were obtained by reducing the nitro group of intermediates **5** and **8** using Pd/C/hydrazine. In addition, model compounds synthetized by thermal imidization of **1** or **2** with phthalic anhydride were successfully prepared (see the ESI† for more details). All target compounds and intermediates were characterized by NMR spectroscopy (^{1}H and ^{13}C), high resolution mass spectrometry (HR-MALDI-MS) and TPA derivative **1** also by X-ray single crystal analysis.

X-Ray single crystal analysis

After slow diffusion of hexane into DCM solution of **1**, a suitable monocrystal for X-ray analysis was obtained. The ORTEP plot in Fig. 2 corresponds to the predicted structure of **1**. It crystallizes in the monoclinic space group $P2_1/c$ bearing eight molecules of **1** along with eight dichloromethane molecules within the unit cell. The core structure resembles the triphenyl- and tris(4-biphenyl)- and tris[4-(4-pyridyl)phenyl]-amines[26–28] found in the Cambridge Structural Database.[29] The nitrogen atoms located between the three phenyl rings are deviated from the planes made by three pivotal carbon atoms (C1, C12 and C23; for one of the molecules shown in Fig. 2) by ∼0.1 Å. The same is expressed in a small difference of ∼2.5° from the ideal value (360°) for the sum of C–N–C angles in the trigonal planar arrangement. The supramolecular arrangement is dominated by H-bond interactions between the NH_2 group and pyridyl nitrogen atoms of neighbouring molecules with NH···N separations of ∼3 Å (see Table S2 and Fig. S15, ESI†). The second pyridyl in the same molecule is bound to the dichloromethane solvent by CH···N interaction (Fig. S15, ESI†). The rest of the atomic distances and angles are found to be in a predictable range.[30]

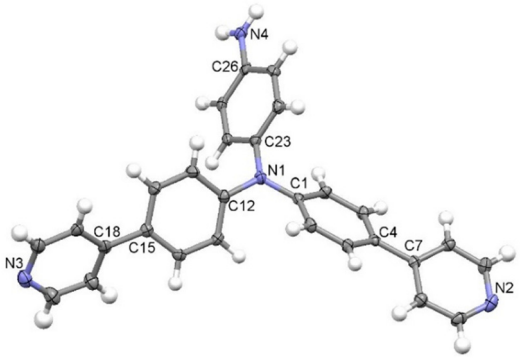

Fig. 2 The molecular structure of **1**. ORTEP diagram with displacement ellipsoids at the 50% probability level. Dichloromethane solvent molecules are omitted for clarity.

Photophysical properties

The optical characteristics of amines **1** and **2** were investigated in DCM and THF, and the measured data are summarized in Table 1 and Fig. 3. The absorption maxima of carbazole **2** were found within the UV area (324/327 nm in DCM/THF; Fig. 3b). On the other hand, TPA chromophore **1** possesses the absorption maxima red-shifted to 369/371 nm with the absorption edges reaching the Vis area (Fig. 3a), which imparts the

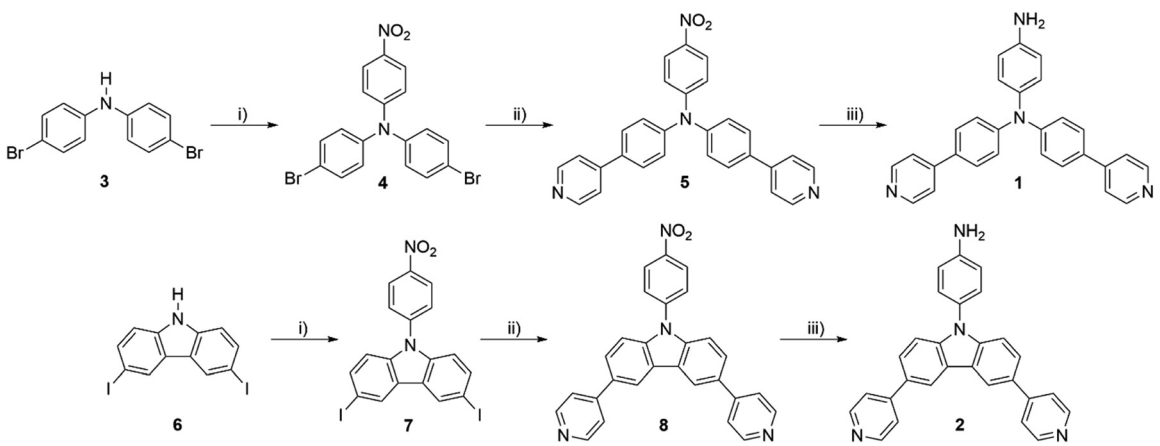

Scheme 1 Synthesis of comonomers **1** and **2**: (i) 1-fluoro-4-nitrobenzene, K_2CO_3, DMSO, 145 °C, 12 h; (ii) pyridine-4-ylboronic acid, $PdCl_2(PPh_3)_2$, Na_2CO_3, dioxane/H_2O (4 : 1), 90 °C, 12 h; (iii) Pd/C, $N_2H_4{\cdot}H_2O$, EtOH, 100 °C, 12 h.

Table 1 Photophysical properties of chromophores **1** and **2**

Compd	Solvent	λ^{A}_{max} [a] [nm (eV)]	ε [10^3 M^{-1} cm^{-1}]	λ^{A}_{max} [nm]	Stokes shift [cm^{-1}]
1	DCM	369 (3.36)	35.0	555	9082
	THF	371 (3.34)	36.4	565	9255
2	DCM	324 (sh) (3.83)	40.3	427	7445
	THF	327 (3.79)	17.4	440	7854

[a] λ^{A}_{max} – the longest-wavelength absorption maxima.

solution of **1** with pale yellow colour. In general, three excitonic transitions are anticipated for tripodal chromophores.[31,32] Whereas flexible TPA derivative **1** has only two low-energy peak maxima (~325/370 nm) with the most intense longest-wavelength absorption band appearing at around 370 nm, rigid carbazole **2** possesses one similar peak at intermediate energy (seen as a shoulder at around 325 nm) and a dominant high-energy peak at ~290 nm. These spectral features are in accordance with the absorption spectra of similar TPA- and carbazole-centred chromophores published in the literature.[33–37] Having the same D–π–D–(π –A)$_2$ arrangement and bearing the same chromophoric units, the spectral difference must be ascribed to the planarized central amino donor in carbazole derivative **2**. Whereas the central nitrogen atom of TPA derivative **1** adopts a tetrahedral arrangement (see Fig. 2), and allows conjugation of the lone electron pair into the appended pyridine-terminated branches, the planarized structure of **2** (Fig. S16, ESI†) diminishes intramolecular charge-transfer to both pyridine acceptors resulting in hypsochromically shifted spectra by about 45 nm.[38]

Both amines **1** and **2** are emissive in DCM and THF (Fig. 3c and d), with the emission maxima within the range of 427 to 565 nm. Whereas rigid **2** showed blue luminescence in both solvents, flexible **1** showed yellowish luminescence in DCM and blue emission in THF. This behaviour reflects their structural features, where **1** most likely undergoes significant structural rearrangement upon excitation as compared to **2**. The measured Stokes shift is higher for **1**, which further corroborates the aforementioned conclusion. In addition to the main fluorescence band, **1** exhibited a second, high-energy emission band at around 420 nm in THF (seen as a shoulder in DCM). This may be assigned to a locally excited state corresponding to electron transition between the peripheral amino donor and TPA core.[39] The low-energy fluorescence band is assigned to electron transition between the TPA core and pyridine acceptors similar to that we have seen in our previous work on TPA derivatives.[26] Increasing the polarity of the media (polarity index P' = 3.1/4.0 for DCM/THF)[40] resulted in red-shifted emission maxima of **1** and **2**.

Electrochemical properties

The electrochemical characterization of target chromophores **1** and **2** was carried out in THF containing 0.1 M Bu_4NPF_6 in a three-electrode cell by cyclic voltammetry (CV). The acquired data are summarized in Table 2, and CV diagrams and further CV description are given in the ESI.†

The first oxidation and reduction processes were primarily captured by voltammetric measurements. These oxidations/

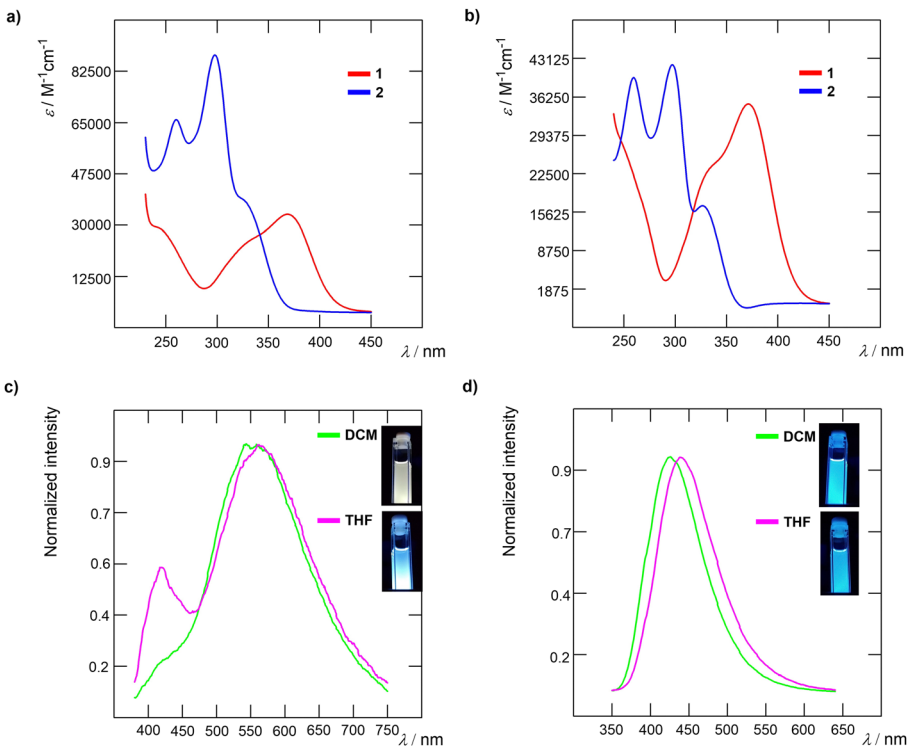

Fig. 3 Absorption spectra of **1** and **2** in (a) DCM and (b) THF. Normalized emission spectra of chromophores in DCM and THF solutions (c) **1** and (d) **2**.

Table 2 Electrochemical and thermal properties of target compounds **1** and **2**

C	$E_{p(ox1)}$[a] [V]	$E_{p(red1)}$[a] [V]	ΔE[a] [eV]	E_{HOMO}[b] [eV]	E_{LUMO}[b] [eV]	T_m[c] (°C)	T_d[d] (°C)	T_i[e] (°C)	$T^{5\%}$[f] (°C)
1	0.76	−2.33	3.09	−5.08	−1.99	—	>460	225	300
2	1.02	−2.36	3.38	−5.34	−1.96	349	>490	215	315

[a] $E_{p(ox1)}$ and $E_{p(red1)}$ are peak potentials of the first oxidation and reduction, respectively, as measured by CV; all potentials are given *vs.* SSCE, $\Delta E = E_{p(ox1)} - E_{p(red1)}$. [b] $-E_{HOMO/LUMO} = (E_{p(ox1)} + 0.036)$ or $(E_{p(red1)} + 0.036) + 4.28$ (*vs.* SCE).[41,42] The increment of +0.036 V corresponds to the difference between SCE (0.241 *vs.* SHE) and SSCE (0.205 *vs.* SHE).[43] [c] T_m = melting point (the point of intersection of a baseline and a tangent of thermal effect = onset). [d] T_d = thermal decomposition (pyrolysis in N_2 atmosphere). [e] T_i = initial temperature of thermal degradation (determined as the last common point of the TGA curve and its first derivation - DTG curve). [f] $T^{5\%}$ = temperature of 5% weight loss (determined by a gradual horizontal step on the TGA curve).

reductions were recorded as irreversible processes, see Fig. S17 (ESI†). The $E_{p(ox1)}$ and $E_{p(red1)}$ values for chromophores **1** and **2** were found within the range of 0.76 to 1.02 and −2.33 to −2.36 V, respectively, and were further recalculated to the HOMO/LUMO levels (Table 2). Despite the fact that the electrochemically derived peak potentials do not correspond in absolute values with the HOMO/LUMO levels (half-wave potentials are not available), these values were used as uniform for describing the electrochemical trends. Assuming the first oxidation as a one-electron process located at the terminal amino donor, according to the anodic/cathodic current maxima, the first reduction was recorded as a multi-electron process (2–3 e^-). This corresponds with the number of pyridine acceptors in the molecule. Multi-electron nature is further confirmed by the presence of a shoulder at E_{sh} = −2.25 V within the first reduction peak of chromophore **2**. However, the potential of the first reduction was related to the peak (current) maxima of these consecutive electron processes.

Thermal properties

Thermal behaviour of chromophores **1** and **2** was studied by differential scanning calorimetry (DSC) and thermogravimetric analysis (TGA). Melting points (T_m) and thermal decomposition temperatures (T_d) were measured by DSC. Initial temperatures of thermal degradation (T_i) and temperatures of 5% weight loss ($T^{5\%}$) were determined by the TGA analysis. All these values are summarized in Table 2.

Target molecules possess high thermal stability as deduced from the DSC records. Compound **2** underwent a melting process (T_m = 349 °C), which was recorded as a typical sharp endothermic peak (Fig. S19, ESI†). Under the ongoing heating program, a gradual endothermic evaporation of the liquid phase was observed. During evaporation, the DSC curve turns into an exothermic process (up to 490 °C), which most likely indicates thermal decomposition. A carbonized residue in the crucible after measurement further confirmed thermal degradation of **2** during the evaporation process. In contrast, a different thermal behaviour was observed for **1**, which does not melt and its solid sample distinctly sublimes above 350 °C. Analogously with molecule **2**, a partial decomposition of the remaining sample **1** occurred at around 460 °C (Fig. S18, ESI†). In addition, a small broad endothermic peak between 120–140 °C was detected for compound **1**, which probably indicates the desorption of residual solvent molecules from the crystal lattice. This probably led to the partial disintegration of the lattice and the formation of an amorphous solid arrangement, which was confirmed by a re-cooling and re-heating process that revealed a glass transition at around 100 °C (Fig. S18, ESI†). These conclusions were further supported by the TGA analysis (Fig. S20a, ESI†). A weight loss of *ca.* 2.5% was captured between 100–200 °C for **1**, which corresponds with the aforementioned desorption of residual solvents. When the samples **1–2** were isothermally held at 30 °C above their T_i, the linear trend in weight loss confirmed their weak sublimation, especially for **1** (Fig. S21, ESI†). Since the TGA analysis was carried out in fully open crucibles (unlike the DSC), compound **1** suffered a significant weight loss (*ca.* 85%) between 300 and 370 °C due to intense sublimation. On the other hand, the significant weight loss of compound **2** is given by the evaporation of the liquid sample after its melting above 350 °C. Nevertheless, more than 40% of carbonized residues after TGA analysis indicates a clear thermal degradation of compound **2**, which can be related to the distinctive shoulder seen in the corresponding DTG curve at around 440 °C (Fig. S20b, ESI†).

DFT Calculations

To obtain further insight into the spatial arrangement and properties of amino comonomers **1** and **2**, DFT calculations were performed by using Gaussian 16 W at the B3LYP/6-311++G(2d,p) level in THF. The optimized geometries were used for all further calculations. The theoretical electronic absorption spectra were calculated at the TD-DFT (nstates = 10) CAM-B3LYP/6-311++G(2d,p) level in THF.[44] Optimized geometries, localization of the frontier molecular orbitals and the energies of the HOMO and LUMO are shown in Fig. 4 and Fig. S23 (ESI†). Whereas TPA chromophore **1** shows a typical propeller-shaped arrangement of phenyls, the phenylamino group in carbazole **2** is almost perpendicular to the carbazole moiety. This structural arrangement affects the electron distribution and thus fundamental properties of both chromophores. In both chromophores, the LUMO (−1.79 eV for **1**, −1.59 for **2**) is similarly spread across the pyridine moieties, while localization of the occupied orbitals is strongly affected by the structure. The twisted phenylamino moiety in carbazole **2** is electronically almost isolated from the rest of the molecule, which results in the localization of the HOMO (−5.84 eV) across the carbazole unit and the HOMO−1 on the phenylamino group. TPA chromophore **1** possesses both the HOMO (−5.27 eV) and the HOMO−1 distributed over all three branches. These structural features are reflected by a

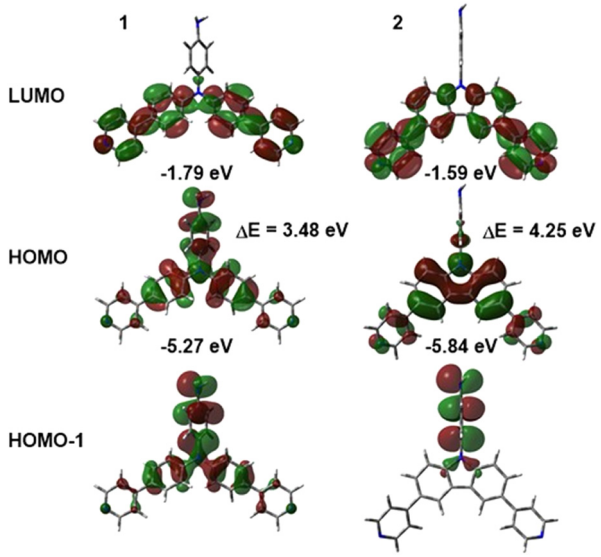

Fig. 4 Visualization of frontier molecular orbitals of chromophores **1** and **2**.

significantly narrowed energy band gap of 3.48 eV calculated for **1**, which is in contrast to 4.25 eV for **2**. These calculated values further corroborate the experimental data obtained from the electrochemical and photophysical measurements. As compared to experimental ones, the calculated electronic absorption spectra are similarly shaped (Fig. S22, ESI†) and slightly blue-shifted (by ca 45 nm), which is consistent with our previous observations.[45] Transition analysis revealed the longest-wavelength band of both **1** and **2** generated by the HOMO → LUMO transition, whereas transitions from the HOMO-2 and the HOMO to higher unoccupied orbitals were identified for the high-energy peaks (Fig. S22, ESI†).

Polyimide films

Synthesis

Utilizing two emissive amino-capped comonomers **1** and **2** and two sets of starting amines/anhydrides (BAPP/CHDA and TFMB/6FDA), four series of emissive PI films were prepared (Scheme 2) along with two non-emissive blanks for comparison. Three amounts of **1** and **2** were used (5, 1 and 0.1 mol %), which afforded three transparent PI materials in each series (Table 3). The PI films were prepared in a two-step reaction sequence involving the synthesis of PAA and its subsequent casting on glass plates and thermal imidization under high vacuum. All prepared PI films were transparent, emissive and flexible except for **PI-2.1b**, which was brittle. A repeated dissolving of **PI-2.1b** produced insoluble microgels and, therefore, it was not further studied. Successfully prepared PI films were analysed using FTIR (see Fig. S24–S27, ESI†). The characteristic bands at around 1780 cm^{-1}, 1720 cm^{-1} and 1370 cm^{-1} corresponding to the C═O asymmetric stretching, C═O symmetric stretching and C–N stretching in the imide moieties, respectively, were evidenced. On the other hand, the absorption peak of C═O in PAA at around 1660 cm^{-1} wasn't observed, confirming complete imidization of the materials.

Photophysical properties

The optical characteristics of the PI films were investigated as summarized in Table 3. All materials, except blanks, are transparent as well as luminescent (see Table S4 for real images, ESI†). Polyimides containing 1 or 5 mol% of amino comonomer **1** are yellowish, while films **PI-1.1c** and **PI-2.1c** containing 0.1 mol% of **1** are colourless. Polyimides containing carbazole-based amino comonomer **2** are colourless except for **PI-1.2a**, which is slightly yellowish. The normalized UV-Vis and photoluminescent (PL) spectra of the target thin films are

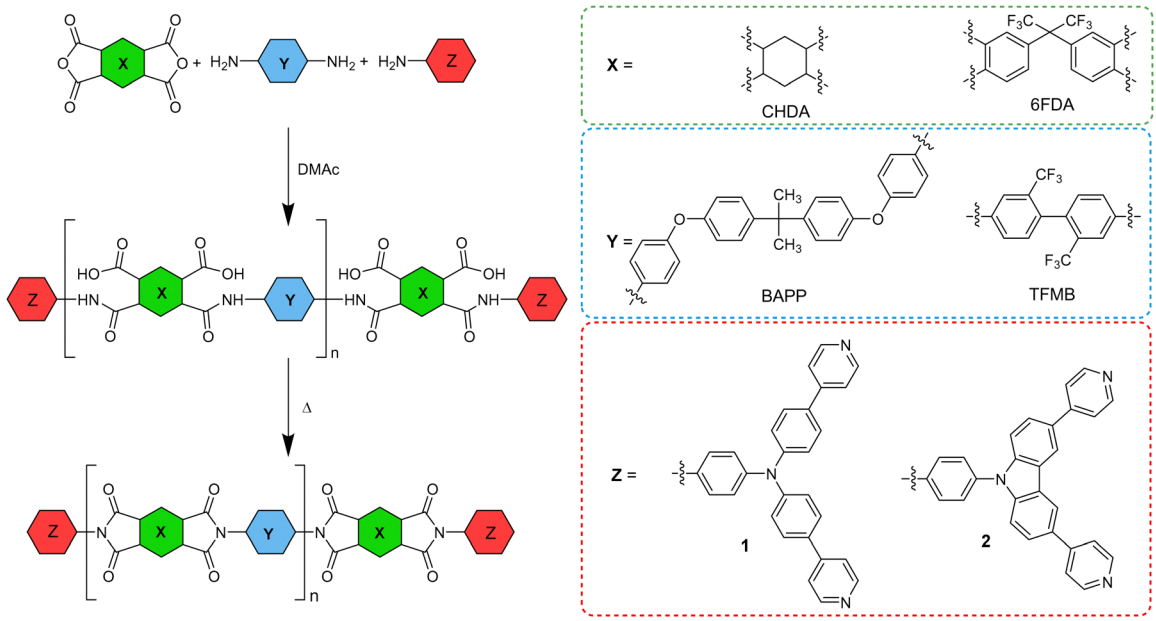

Scheme 2 General synthesis of end-capped polyimides.

Table 3 Composition, visual and photophysical properties of PI films

Polymer	Amine	Anhydride	Comon.	Mol. [%]	Emission	Colour	$\lambda_{cut\text{-}off}$ [nm][b]	T^{400} [%][c]	T^{700} [%][c]	λ^{A}_{max} [nm]	λ^{xE}_{ma} [nm]	Chromaticity CIE[d] (x, y)	FWHM [nm]
PI-1	TFMB	6FDA	—	—	NO	Colourless	348	81	90	—	—	—	—
PI-2	BAPP	CHDA	—	—	NO	Colourless	295	86	91	—	—	—	—
PI-1.1a	TFMB	6FDA	**1**	5	YES	Yellowish	393	5	90	418	588	0.487, 0.470	129
PI-1.1b	TFMB	6FDA	**1**	1	YES	sl. yellowish	369	48	90	405	580	0.438, 0.472	135
PI-1.1c	TFMB	6FDA	**1**	0.1	YES	Colourless	354	72	90	398	509	0.308, 0.399	160
PI-2.1a	BAPP	CHDA	**1**	5	YES	sl. yellowish	392	10	89	410	427	0.211, 0.234	117
PI-2.1b	BAPP	CHDA	**1**	1	YES	—[a]	—[a]	—[a]	—[a]	—[a]	—[a]	—[a]	—[a]
PI-2.1c	BAPP	CHDA	**1**	0.1	YES	Colourless	298	75	89	400	410	0.162, 0.044	54
PI-1.2a	TFMB	6FDA	**2**	5	YES	sl. yellowish	365	33	89	455	518	0.322, 0.485	121
PI-1.2b	TFMB	6FDA	**2**	1	YES	Colourless	353	72	90	443	504	0.274, 0.421	117
PI-1.2c	TFMB	6FDA	**2**	0.1	YES	Colourless	352	77	90	378	502	0.277, 0.386	127
PI-2.2a	BAPP	CHDA	**2**	5	YES	Colourless	354	73	88	367	383	0.178, 0.164	48
PI-2.2b	BAPP	CHDA	**2**	1	YES	Colourless	333	82	89	360	381	0.166, 0.054	38
PI-2.2c	BAPP	CHDA	**2**	0.1	YES	Colourless	295	86	90	356	380	0.173, 0.106	42

[a] Brittle. [b] Cut-off wavelength. [c] T^{400}, T^{700}: transmittance at 400/700 nm of average 50 μm thick film. [d] CIE coordinates of the emission spectra calculated according to ref. 46.

displayed in Fig. 5. Normalized absorption spectra of PI films show the same shape and differ in the position of the absorption band and onset absorption band, that shift hypsochromically with decreasing amount of comonomer **1** (*e.g.* $\Delta\lambda$ = 70 nm when going from **PI-1.2a** to **PI-1.2c**; Fig. 5b). This observation is in accordance with the decreasing molecular weight within the order of $c \rightarrow b \rightarrow a$. The photoluminescence spectra are composed of one emission peak found within the region of 350–700 nm, which is red-shifted upon increasing the molar ratio of **1** and **2**. As compared to the emission of **1** and **2** in solution, PI-films containing a TFMB-6FDA core possess bathochromically shifted emission, while the emission bands of BAPP-CHDA films are shifted hypsochromically. When compared to the emission of model imides **MC-1** and **MC-2** (see the ESI†), the emission maxima of both films are generally red-shifted. This phenomenon was observed earlier.[24] When comparing the polyimide cores, TFMB-6FDA *vs.* BAPP-CHDA, films made of the latter possess significantly blue-shifted emission (*e.g.* λ^{E}_{max} = 518/383 nm for **PI-1.2a**/**PI-2.2a**), which can be ascribed to the fluorinated TFMB-6FDA aromatic structure *vs.* semi-aliphatic BAPP-CHDA. When considering general interest in blue emitters featuring $CIE_y \leq 0.1$ and high colour purity,[47,48] BAPP-CHDA films with **2**, namely **PI-2.2b** and **PI-2.2c** with CIE coordinates of (0.166, 0.054) resp. (0.173, 0.106) (Fig. 7) and very narrow full-width half-maximum (FWHM; 38 resp. 42 nm), are considered as very promising blue emitting polymeric materials (Table 3).

Transmittance of PI films (Table 3) strongly depends on the wavelength (400 and 700 nm), type of PI film and amount of the chromophores **1** and **2** (Fig. 6). Increasing concentration of **1** or **2** increased $\lambda_{cutt\text{-}off}$ and decreased T^{400}. This effect is most pronounced when going from **a** to **c** within the series **PI-1.1**, where transmittance ranges from 5 to 72%. All PI films are well transparent at 700 nm (T^{700} = 88 to 91%). Blue-shifted

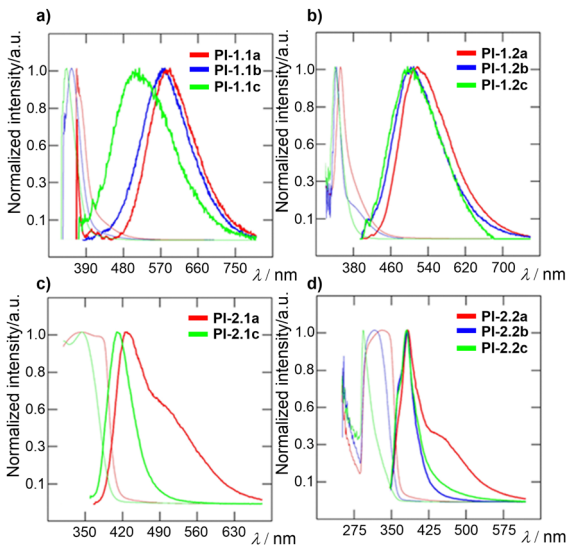

Fig. 5 Absorption (thin line) and emission (bold line) spectra of PI thin films.

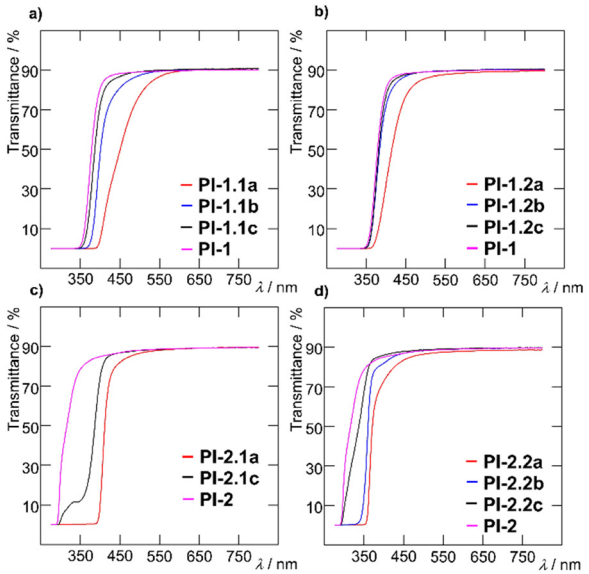

Fig. 6 Transmittance of PI films.

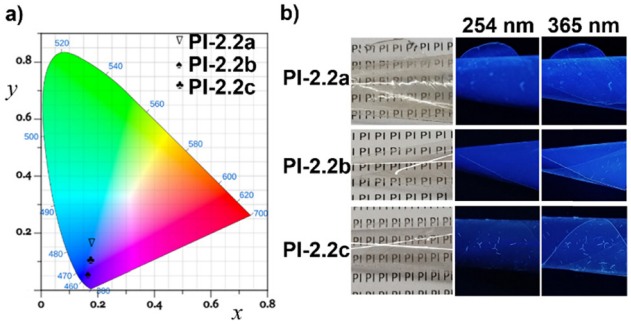

Fig. 7 (a) CIE chromaticity diagram 1931 of emissive PI film series **PI2.2a–c**,[46] (b) photographs of PI films under ambient light and a hand-held UV lamp (254 and 365 nm).

absorption of **2**, in respect to **1**, brings also higher transparency of carbazole-terminated polymers at 400 nm (Fig. 6).

Thermal properties

Thermal properties of PI films were investigated by DSC and TGA (Table 4 and Fig. S30 and S31, ESI†). Thermal robustness is mostly dictated by the polyimide backbone, and aromatic TFMB-6FDA proved to be more thermally robust as compared to aliphatic BAPP-CHDA (*e.g.* $\Delta T^{5\%} = 57$ °C). On the other hand, the effect of comonomer **1** or **2** is diminished, *e.g.* a slight improvement is seen when comparing doped and unmodified PI films **PI-1** and **PI-2** ($T^{5\%} = 526/511$ °C for **PI-1.2c**/**PI-1**). This effect is ascribed to PI films terminated by more thermally robust aromatic compounds **1** or **2**. Higher thermal robustness of carbazole-terminated films further corroborates this supposition. On the contrary, increasing amount of **1** and **2** shortens the PI chain and reduces the $T^{5\%}$ and T_g values.

Experimental

Detailed synthetic and experimental procedures, and additional data concerning all materials and instrumentation used for separation, isolation and analysis for this article have been included in the ESI.†

Table 4 Thermal properties of PI films

Polymer	$T^{5\%}$ $(N_2)^a$ [°C]	$T^{10\%}$ $(N_2)^a$ [°C]	Char yield[b] [%]	$T_g{}^c$ [°C]
PI-1	511	531	60	327
PI-2	454	470	30	258
PI-1.1a	510	531	62	306
PI-1.1b	515	535	65	317
PI-1.1c	516	536	62	325
PI-2.1a	455	464	39	262
PI-2.1b	—[d]	—[d]	—[d]	—[d]
PI-2.1c	458	471	34	252
PI-1.2a	524	545	67	304
PI-1.2b	524	547	72	323
PI-1.2c	526	545	70	332
PI-2.2a	457	470	43	265
PI-2.2b	448	463	31	260
PI-2.2c	454	473	38	265

[a] $T^{5\%}$ and $T^{10\%}$ are temperatures of 5 and 10% weight loss, respectively. [b] Char yield after TGA analysis at 600 °C under N_2 atmosphere. [c] T_g means glass transition temperature measured by DSC. [d] Brittle.

Conclusions

Two new emissive chromophores and their utilization as comonomers for the preparation of emissive polyimides are reported. The chromophores were based on triphenylamine and a carbazole central unit. As compared to tetrahedral triphenylamine **1**, the partially planarized/rigid structure of carbazole **2** brings different photophysical and thermal properties. Its absorption has been found fully in the near UV area, which is promising for the production of a transparent PI film. The thermal stability of the carbazole chromophore is also improved. Semi-aliphatic polyimides (CHDA-BAPP) and fluorinated aromatic polyimides (6FDA-TFMB) were combined with amino-capped comonomers **1** and **2** (5, 1 or 0.1 mol%) to afford various emissive PI films. Except for one film, all the prepared polyimides were shown to be flexible, transparent, and luminescent with high thermal stability; six of the PI films were colourless. Their fundamental properties can be easily tuned by a proper combination of PI backbone and comonomer. Fluorinated aromatic PIs possess red-shifted emission maxima as compared to semi-aliphatic ones (CHDA-BAPP), especially TPA-terminated ones (series **PI-1.1a–PI-1.1c**). On the contrary, semi-aliphatic polyimides prepared from CHDA-BAPP are more optically transparent but possess lower thermal stability and T_g as compared to fluorinated polyimides. Semi-aliphatic carbazole-terminated PIs (films **PI-2.2b–PI-2.2c**) showed excellent optical properties with $CIE_y \leq 0.1$ and high colour purity determined by FWHM 38 resp. 42 nm and, therefore can be considered as interesting blue emitters. In summary, carbazole-terminated PIs showed better trade-off between optical transparency and thermal stability.

Author contributions

J. T.: conceptualization. P. Š., J. Š., M. K., Z. B., A. R.: investigation. J. T., P. Š., M. K., Z. B., A. R.: writing – original draft. J. Z., J. K.: supervision. J. T.: writing – review & editing.

Conflicts of interest

There are no conflicts to declare.

Acknowledgements

This work was supported by European Regional Development Fund-Project " High sensitive sensors and low-density materials based on polymeric nanocomposites – NANOMAT (No. CZ.02.1.01/0.0/0.0/17_048/0007376)".

Notes and references

1 J. Roncali, P. Leriche and P. Blanchard, *Adv. Mater.*, 2014, **26**, 3821–3838.

2 F. Mateen, T. G. Hwang, L. F. Boesel, W. J. Choi, J. P. Kim, X. Gong, J. M. Park and S. K. Hong, *Int. J. Energy Res.*, 2021, **45**, 17971–17981.
3 C. Papucci, T. A. Geervliet, D. Franchi, O. Bettucci, A. Mordini, G. Reginato, F. Picchioni, A. Pucci, M. Calamante and L. Zani, *Eur. J. Org. Chem.*, 2018, 2657–2666.
4 W. Z. Yuan, Y. Gong, S. Chen, X. Y. Shen, J. W. Y. Lam, P. Lu, Y. Lu, Z. Wang, R. Hu, N. Xie, H. S. Kwok, Y. Zhang, J. Z. Sun and B. Z. Tang, *Chem. Mater.*, 2012, **24**, 1518–1528.
5 C. Y. Chan, M. Tanaka, Y. T. Lee, Y. W. Wong, H. Nakanotani, T. Hatakeyama and C. Adachi, *Nat. Photonics*, 2021, **15**, 203–207.
6 S. O. Jeon, K. H. Lee, J. S. Kim, S. G. Ihn, Y. S. Chung, J. W. Kim, H. Lee, S. Kim, H. Choi and J. Y. Lee, *Nat. Photonics*, 2021, **15**, 208–215.
7 X. Liu, X. Wei, Y. Miao, P. Tao, H. Wang and B. Xu, *Tetrahedron*, 2021, **86**, 132061.
8 N. Jiang, B. Wang, T. Liu, Q. Liu, Q. Wei, Y. Xing and G. Zheng, *Anal. Methods*, 2019, **11**, 232–235.
9 Y. Gu, R. Yuan, X. Yan, C. Li, W. Liu, R. Chen, L. Tang, B. Zheng, Y. Li, Z. Zhang and M. Yang, *Anal. Chim. Acta*, 2015, **889**, 113–122.
10 S. Wu, H. Song, J. Song, C. He, J. Ni, Y. Zhao and X. Wang, *Anal. Chem.*, 2014, **86**, 5922–5928.
11 X. Wang, G. Ding, Y. Wang, S. Mao, K. Wang, Z. Ge, Y. Zhang, X. Li and C. H. Hung, *Tetrahedron*, 2020, **76**, 131726.
12 T. G. Hwang, J. Y. Kim, J. W. Namgoong, J. M. Lee, S. B. Yuk, S. H. Kim and J. P. Kim, *Photochem. Photobiol. Sci.*, 2019, **18**, 1064–1074.
13 Y. Kuramoto, T. Nakagiri, Y. Matsui, E. Ohta, T. Ogaki and H. Ikeda, *Photochem. Photobiol. Sci.*, 2018, **17**, 1157–1168.
14 P. Pander, R. Motyka, P. Zassowski, M. K. Etherington, D. Varsano, T. J. Da Silva, M. J. Caldas, P. Data and A. P. Monkman, *J. Phys. Chem. C*, 2018, **122**, 23934–23942.
15 J. Moon Lee, S. Bum Yuk, J. Woong Namgoong and J. Pil Kim, *Dyes Pigm.*, 2021, **185**, 108864.
16 I. Gouzman, E. Grossman, R. Verker, N. Atar, A. Bolker and N. Eliaz, *Adv. Mater.*, 2019, **31**, 1807738.
17 H. Ni, J. Liu, Z. Wang and S. Yang, *J. Ind. Eng. Chem.*, 2015, **28**, 16–27.
18 T. Xiao, X. Fan, D. Fan and Q. Li, *Polym. Bull.*, 2017, **74**, 4561–4575.
19 A. Tabuchi, T. Hayakawa, S. Kuwata, R. Ishige and S. Ando, *Polymers*, 2021, **13**, 4050.
20 K. Kanosue, S. Hirata, M. Vacha, R. Augulis, V. Gulbinas, R. Ishige and S. Ando, *Mater. Chem. Front.*, 2019, **3**, 39–49.
21 K. Kanosue, R. Augulis, D. Peckus, R. Karpicz, T. Tamulevičius, S. Tamulevičius, V. Gulbinas and S. Ando, *Macromolecules*, 2016, **49**, 1848–1857.
22 S. H. Lee, J. Bae, H. M. Seo, J. H. Im, H. S. Shin, E. J. Yoo and S. W. Lee, *Mol. Cryst. Liq. Cryst.*, 2014, **598**, 6–15.
23 C. H. Chang, K. L. Wang, J. C. Jiang, D. J. Liaw, K. R. Lee, J. Y. Lai and K. H. Lai, *Polymer*, 2010, **51**, 4493–4502.
24 A. Iqbal, N. Khalid, H. M. Siddiqi, O. O. Park and T. Akhter, *J. Fluoresc.*, 2018, **28**, 311–321.
25 J. Tydlitát, M. Fecková, P. le Poul, O. Pytela, M. Klikar, J. Rodríguez-López, F. Robin-le Guen and S. Achelle, *Eur. J. Org. Chem.*, 2019, 1921–1930.
26 J. Tydlitát, S. Achelle, J. Rodríguez-López, O. Pytela, T. Mikýsek, N. Cabon, F. Robin-le Guen, D. Miklík, Z. Růžičková and F. Bureš, *Dyes Pigm.*, 2017, **146**, 467–478.
27 L. Cao, L. Zhou, G.-H. Kang, C.-S. Ruan and B.-M. Ji, *Z. Kristallogr. – New Cryst. Struct.*, 2013, **228**, 329–330.
28 B. Mondal, K. Acharyya, P. Howlader and P. S. Mukherjee, *J. Am. Chem. Soc.*, 2016, **138**, 1709–1716.
29 C. R. Groom, I. J. Bruno, M. P. Lightfoot and S. C. Ward, *Acta Crystallogr., Sect. B: Struct. Sci., Cryst. Eng. Mater.*, 2016, **72**, 171–179.
30 F. H. Allen, D. G. Watson, L. Brammer, A. G. Orpen and R. Taylor, *Int. Tables Crystallogr.*, 2006, 790–811.
31 K. Seintis, I. K. Kalis, M. Klikar, F. Bureš and M. Fakis, *Phys. Chem. Chem. Phys.*, 2020, **22**, 16681–16690.
32 H. Ceymann, M. Balkenhohl, A. Schmiedel, M. Holzapfel and C. Lambert, *Phys. Chem. Chem. Phys.*, 2016, **18**, 2646–2657.
33 X. Du, J. Zhao, W. Liu, K. Wang, S. Yuan, C. Zheng, H. Lin, S. Tao and X. H. Zhang, *J. Mater. Chem. C*, 2016, **4**, 10301–10308.
34 K. Yu, J. Pan, M. Tian, H. Zhang, C. Jin, H. Zhang, Z. Mao and Q. He, *Chem. – Asian J.*, 2022, **17**, e202200571.
35 A. R. Marri, F. A. Black, J. Mallows, E. A. Gibson and J. Fielden, *Dyes Pigm.*, 2019, **165**, 508–517.
36 Y. L. Zhang, Q. Ran, Q. Wang, Q. S. Tian, F. C. Kong, J. Fan and L. S. Liao, *Org. Electron.*, 2020, **81**, 105660.
37 W. W. Tao, K. Wang, J. X. Chen, Y. Z. Shi, W. Liu, C. J. Zheng, Y. Q. Li, J. Yu, X. M. Ou and X. H. Zhang, *J. Mater. Chem. C*, 2019, **7**, 4475–4483.
38 A. Vogel, T. Schreyer, J. Bergner, F. Rominger, T. Oeser and M. Kivala, *Chem. – Eur. J.*, 2022, **28**, e202201424.
39 M. D. Zhang, Z. Q. Shi, M. D. Chen and H. G. Zheng, *Dalton Trans.*, 2015, **44**, 5818–5825.
40 L. R. Snyder, *J. Chromatogr. Sci.*, 1978, **16**, 223–234.
41 T. J. Carter, R. Mohtadi, T. S. Arthur, F. Mizuno, R. Zhang, S. Shirai and J. W. Kampf, *Angew. Chem., Int. Ed.*, 2014, **53**, 3173–3177.
42 A. A. Isse and A. Gennaro, *J. Phys. Chem. B*, 2010, **114**, 7894–7899.
43 D. T. Sawyer, A. Sobkowiak and J. L. Roberts, *Electrochemistry for chemists*, J. Wiley and Sons Inc., 2nd edn, 1995.
44 M. J. Frisch, G. W. Trucks, H. B. Schlegel, G. E. Scuseria, M. A. Robb, J. R. Cheeseman, G. Scalmani, V. Barone, G. A. Petersson, H. Nakatsuji, X. Li, M. Caricato, A. V. Marenich, J. Bloino, B. G. Janesko, R. Gomperts, B. Mennucci, H. P. Hratchian, J. V. Ortiz, A. F. Izmaylov, J. L. Sonnenberg, D. Williams-Young, F. Ding, F. Lipparini, F. Egidi, J. Goings, B. Peng, A. Petrone, T. Henderson, D. Ranasinghe, V. G. Zakrzewski, J. Gao, N. Rega, G. Zheng, W. Liang, M. Hada, M. Ehara, K. Toyota, R. Fukuda, J. Hasegawa, M. Ishida, T. Nakajima, Y. Honda, O. Kitao, H. Nakai, T. Vreven, K. Throssell, J. A. Montgomery, Jr., J. E. Peralta, F. Ogliaro,

M. J. Bearpark, J. J. Heyd, E. N. Brothers, K. N. Kudin, V. N. Staroverov, T. A. Keith, R. Kobayashi, J. Normand, K. Raghavachari, A. P. Rendell, J. C. Burant, S. S. Iyengar, J. Tomasi, M. Cossi, J. M. Millam, M. Klene, C. Adamo, R. Cammi, J. W. Ochterski, R. L. Martin, K. Morokuma, O. Farkas, J. B. Foresman and D. J. Fox, *Gaussian 16*, Gaussian, Inc., Wallingford CT, 2019.

45 M. Klikar, D. Georgiou, I. Polyzos, M. Fakis, Z. Růžičková, O. Pytela and F. Bureš, *Dyes Pigm.*, 2022, **201**, 110230.

46 E. H. H. Hasabeldaim, CIE chromaticity diagram 1931, 2021, **https://sciapps.sci-sim.com/CIE1931.html**.

47 M. Xie, M. Sun, S. Xue and W. Yang, *Dyes Pigm.*, 2022, **208**, 110799.

48 X. Yang, X. Xu and G. Zhou, *J. Mater. Chem. C*, 2015, **3**, 913–944.